Original Paper *Forma*, **15**, 291–308, 2000

Complex Dynamical Response of Chemical and Biochemical Excitable Systems to Periodic Stimuli

Vladislav NEVORAL, Michal VOSLAŘ, Igor SCHREIBER, Pavel HASAL and Miloš MAREK

Department of Chemical Engineering and Center for Nonlinear Dynamics of Chemical and Biological Systems, Institute of Chemical Technology, Prague, CZ-166 28 Prague 6, Czech Republic
E-mail: Vladislav.Nevoral@vscht.cz, Michal.Voslar@vscht.cz, Igor.Schreiber@vscht.cz, Pavel.Hasal@vscht.cz, Milos.Marek@vscht.cz

(Received April 19, 2000; Accepted May 19, 2000)

Keywords: Coupled Cells, Excitability, Chaos, Intercellular Signalling, Electric Field Effects

Abstract. Excitable properties of selected biochemical reactions in one compartment subject to external periodic stimuli, the spreading of signals elicited by periodic stimulation in a linear array of compartments and the spreading of pulse wave trains in a continuous medium are studied. A method of calculating a threshold set and a criterion for its disappearance are formulated. Two kinds of excitability distinguished by either direct or indirect initiation of the activatory process are discussed. The response of the one- and two-compartment systems to periodic perturbations is studied upon varying a bifurcation parameter. Transitions from periodicity to quasiperiodicity and to chaos are observed. The problem of intercellular signalling is addressed by observation of an excitable pulse propagation in reaction-diffusion media with an oscillatory pacemaker entrapped within the excitable domain. The signalling patterns are analysed by proper orthogonal decomposition based techniques and effects of electric field applied to the system are examined.

1. Introduction

Biochemical processes within the cell environment may serve a host of different purposes. Of particular interest here are excitable processes whose dynamics are sensitive to perturbations. There are many examples of excitable systems in chemistry and biology (HOLDEN *et al*., 1991), ranging from the Belousov-Zhabotinsky chemical reaction (FIELD and BURGER, 1990) to calcium spiking in many types of cells (GOLDBETER, 1996) to action potentials in specialized neural cells (HODGKIN and HUXLEY, 1954). A typical excitatory event follows a superthreshold stimulus applied to the system at rest which triggers an autocatalytic increase of some intermediate(s) until an inhibitory decay dominates, leading eventually to the original rest state. Stimulus may be repeated periodically, either by externally controlled conditions (such as drug administration) or by some internal oscillatory process in the neighborhood of the cell transduced inside or an oscillatory subsystem within the cell. Periodic forcing induces repeated firings which may or may not catch up with the

pace of stimuli depending on the strength and period of the stimulus. The dynamics may become complex when the cell is unable to respond by an excitation to each external stimulus (VOTRUBOVÁ *et al.*, 1998, HASAL *et al.*, 1996, SCHREIBER *et al.* 1999). Apart from neurons, intercellular signalling is known to occur in various cell systems (COOPER, 1995; BOITANO *et al.*, 1992).

Propagation of Ca^{2+} waves through cell assemblages is known to occur in a large number of tissues (BERRIDGE *et al.*, 1998). Increases in the intracellular calcium concentration that spread from cell to cell—*the calcium waves*—form a versatile tool for coordination of many cell activities. Cell-to-cell propagating calcium signals can be evoked by a variety of stimuli, including chemical, mechanical and electric stimulation. The cells in a tissue may exhibit various responses to the stimulation. The cell can start to oscillate, to perform single or repeated firings or it may remain in its original state etc. The actual cell response depends on local external constraints, e.g., concentration of chemical species, local electric potential gradient, local mechanical stress and also on cell history.

In the first part of the paper we examine systematically dynamical response of one biochemical cell to pulsed external forcing provided that the process of interest within the cell—calcium dynamics—is excitable. We find that the degree of dynamic complexity depends on the type of excitability and on the strength of the excitatory event. Diffusion-like coupling of two cells increases further the complexity of the pattern if the coupling strength is appropriately adjusted.

When a cell (or a group of cells) in the tissue is set to the oscillatory state it starts to perturb the neighboring cells via chemical communication (chermical species exchange) through the gap junctions connecting the cells (BOITANO *et al.*, 1992). In this case the periodic perturbation imposed by the oscillating cell(s) results in an oscillatory response of the stimulated cells in a form of pulse waves propagating through the tissue. This issue is analyzed in the second part of this paper.

2. Chaotic Dynamics in Periodically Pulsed Cell Systems

2.1. Model equations

Here we shall use a model of intracellular calcium dynamics according to the one-pool variant of the CICR mechanism (DUPONT and GOLDBETER, 1993). Dynamics of calcium in cells is ubiquitous in animal cells and displays both oscillatory and excitatory modes. However, other biochemical excitable systems, e.g. the papain system (CAPLAN *et al.*, 1973), show the same kind of behavior when periodically perturbed. According to the CICR (Calcium-Induced Calcium Release) model, the key species are the inositol 1, 4, 5-trisphosphate (IP_3), the cytosolic Ca^{2+}(Ca_i) and the calcium ions sequestered in an intracellular store (Ca_s). From a mechanistic viewpoint, Ca_i is the autocatalytic species, Ca_s plays a regulatory role, IP_3 controls the system as a constraint.

In the absence of a mass transport within the cell the dynamics is governed by the mass balance equations

$$\frac{dx}{dt} = f(x, y) = V_{\text{in}} - V_2 + V_3 + k_f y - kx, \tag{1}$$

$$\frac{dy}{dt} = g(x,y) = V_2 - V_3 - k_f y, \tag{2}$$

where

$$V_{\text{in}} = v_0 + v_1\beta, \quad V_2 = V_{M2}\frac{x^n}{\left(K_2^n + x^n\right)}, \quad V_3 = \beta V_{M3}\frac{y^m}{\left(K_R^m + y^m\right)}\frac{x^p}{\left(K_A^p + x^p\right)}, \tag{3}$$

and x is the concentration of Ca_i, y is the concentration of Ca_s, V_{in} is total constant entry of Ca^{2+} into the cytosol consisting of v_0, the constant influx and $v_1\beta$, the IP_3-stimulated influx from extracellular medium, V_2 is the rate of pumping into the internal store, V_3 is the rate of release from the store, k_f is the coefficient of the passive efflux from the store, k is the rate coefficient of the passive efflux from the cytosol. The saturation parameter β represents the regulatory role of IP_3. In all the calculations we use the values given in Table 1. In order to find excitable conditions we treat v_0 and β as adjustable parameters to set appropriate dynamics.

2.2. Excitability

The region of periodic oscillations shown in Fig. 1 is marked by the Hopf bifurcation curve. In fact, this bifurcation is mostly subcritical and thus the oscillations occur also outside this region. However, the additional region of hysteresis is negligibly narrow. As indicated in Fig. 1 we find two different kinds of excitability in this system. The first one, which we call the *activatory excitability*, is associated with a low-*x*-high-*y* steady state. Addition of *x* or *y* triggers the usual excitatory event beginning with the activatory (or autocatalytic) phase which increases *x* and depletes *y* until the inhibitory phase sets in to consume *x* and replete y. The other, somewhat counterintuitive type—*inhibitory excitability*—is associated with a high-*x*-low-*y* steady state. The excitation elicited by removing *x* or *y* begins with the inhibitory process which removes *x* even more and simultaneously repletes *y*, and terminates by the autocatalysis. Another classification of excitable systems distinguishes between multiple steady state (type I) and single steady state (type II) phase portraits (MAREK *et al.*, 1989); in the present case we have a unique steady state and therefore the type II excitability.

To draw the boundaries along which excitability vanishes requires a quantitative rather than qualitative definition of this phenomenon. We consider a threshold set as locally

Table 1. Parameter values for the CICR model.

Par.		Value		Par.		Value		Par.		Value
k_f	=	1.0	min^{-1}	K_2	=	0.5	μM	n	=	2.0
k	=	10.0	min^{-1}	V_{M3}	=	325.0	$\mu\text{M min}^{-1}$	m	=	2.0
v_1	=	1.7	$\mu\text{M min}^{-1}$	K_R	=	1.0	μM	p	=	4.0
V_{M2}	=	50.0	$\mu\text{M min}^{-1}$	K_A	=	0.45	μM			

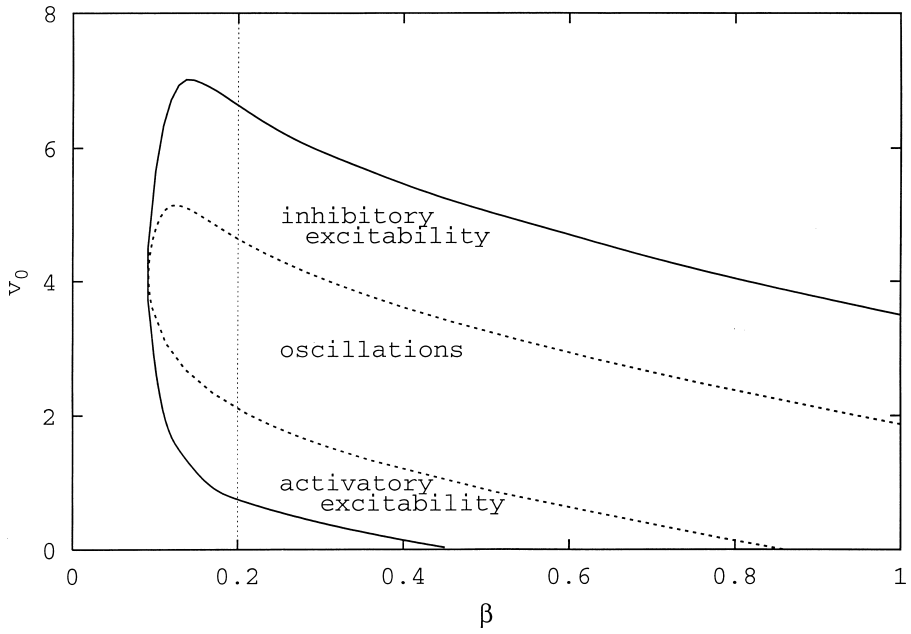

Fig. 1. Bifurcation diagram in the parameters v_0 and β, dashed line—Hopf bifurcation, full line—vanishing excitability.

separating the phase space into a set of trajectories amplifying initial perturbations and a set of trajectories decaying to the steady state soon after the perturbation. For the type I excitability, the threshold set is essentially a stable manifold of a saddle steady state which can be easily identified. This is not possible for the type II excitability and so the threshold set should be chosen in an appropriate way. More specifically, the threshold set should be a codimension one continuous set of trajectory segments possessing two properties: a) there is a minimal and a maximal point on each trajectory segment within the threshold set such that the former is the nearest and the latter is the most distant point relative to the steady state—this provides a measure of amplification; the threshold set terminates at the locus of maximal points, b) the separation of nearby trajectories from the threshold set should be at a maximum possible rate providing thus a distinct boundary between excitatory and nonexcitatory responses.

The two-variable system (1), (2) has a one-dimensional threshold set. Since we have type II excitability we are looking for a trajectory segment. For a general two-variable system described by $d\mathbf{x}/dt = \boldsymbol{v}(\mathbf{x})$ let $\mathbf{x}_S$ be the steady state, $\mathbf{x}_P$ the minimal and $\mathbf{x}_R$ the maximal point on a trajectory. The point $\mathbf{x}_P$ is thought as the state immediately after a pulsed perturbation from the steady state. The perturbation and response amplitudes are

$$P = \left\|\mathbf{x}_P - \mathbf{x}_S\right\|, \qquad R = \left\|\mathbf{x}_R - \mathbf{x}_S\right\| \tag{4}$$

and hence P is a minimal possible pulse amplitude to reach the trajectory with the maximal response at $\mathbf{x}_R$. Next we define an amplification ratio,

$$r = \frac{R - P}{P}. \tag{5}$$

The threshold trajectory is found by requiring maximal possible rate of separation of nearby trajectories which is expressed as maximum sensitivity of the amplification ratio with respect to P,

$$\frac{dr}{dP} \overset{!}{=} \max. \tag{6}$$

A variational principle used to formulate and solve the associated boundary value problem for the threshold set will be discussed elsewhere.

As the parameters v_0 and β approach the outer boundary in Fig. 1, the perturbation amplitude increases, the threshold set shrinks and its separation properties weaken. The excitability of the system may vanish in two ways, either the amplification drops below the limiting value of $r = 1$, or the maximum of dr/dP disappears by coliding with a minimum. Which one is the case depends on the model—the former is the actual mechanism for the CICR model. Similar quantities as r may be defined but all give very similar results.

2.3. Periodic forcing of one cell

We assume that the concentration of Ca_i can be changed suddenly as a consequence of a periodically repeated external perturbation. This can be modelled as a periodic series of delta pulses shifting immediately the value of x and Eqs. (1) and (2) now become

$$\frac{dx}{dt} = f(x, y) + h(x) \sum \delta(t - kT), \qquad k = 1, \ \ldots, \tag{7}$$

$$\frac{dx}{dt} = g(x, y), \tag{8}$$

where k counts the number of pulses, T is the period of pulse deliveries and $h(x)$ is the change in x due to the pulse. When addition of Ca_i is considered, this function is chosen to be simply a constant, $h(x) = A$. However, removal of Ca_i modelled in this way might shift x to negative values and thus we choose $h(x) = x(e^{-A} - 1)$. In both cases we call A the forcing amplitude.

We examine the system (7), (8) numerically by using continuation method (KUBÍČEK and MAREK, 1983; MAREK and SCHREIBER, 1995) to find variations of periodic solutions with A and/or T, their stability and bifurcations. In addition, we also solve Eqs. (7) and (8) directly and charaterize the complexity of dynamics by Poincare maps and Lyapunov exponents. Moreover, the excitatory dynamics is well characterized by introducing excitation (or firing) number v,

$$\nu = \frac{\text{number of excitatory responses}}{\text{number of pulses}} \tag{9}$$

in the limit of large number of pulses k. Thus ν is an average number of excitations per one pulse. Here we can conveniently use the notion of the threshold set introduced earlier to distinguish between excitatory and nonexcitatory repsonses. A response is considered as excitatory if the pulse penetrates the threshold set or, equivalently, if the trajectory loops around the endpoint of the threshold set. Periodic orbits have $\nu = p/q$ where p, q are integers and qT is the period. For further calculations we fix β at 0.2 and examine the dynamics of the forced system at various values of v_0 within the two regions of excitability (cf. Fig. 1).

Figures 2a and 2b show the A–T bifurcation diagrams of the period one orbit at v_0 = 1.2 and v_0 = 5.0. There are instabilities due to the fold bifurcation, period doubling and torus bifurcation. The corresponding unstable regions suggest where the dynamics will likely become complex. Also, the threshold perturbation amplitude for the period one orbit to

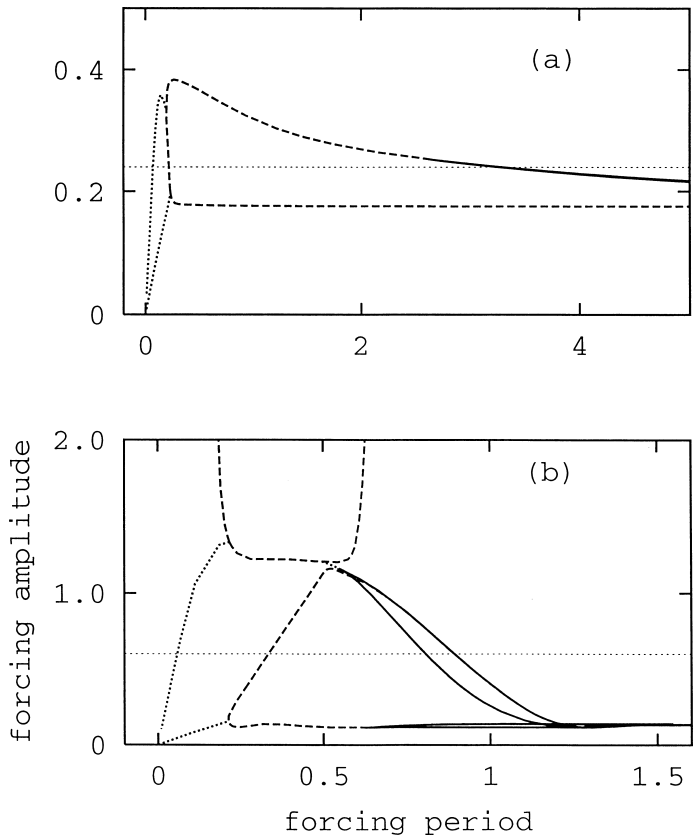

Fig. 2. Bifurcation diagrams for period one orbit in the parameters T and A; (a) v_0 = 1.2, (b) v_0 = 5.0; full line—fold bifurcation, dashed line—period doubling, dotted line—torus bifurcation.

become unstable is nearly constant for large T as one might expect but decreases rapidly when T becomes smaller. Let us remark that analogous calculations for v_0 below the boundary for activatory excitability and above the boundary for the inhibitory excitability show that these bifurcation structures shrink and disintegrate almost completely and thus suggest that the criteria (5), (6) used for constructing the boundary have significant predictive power.

Figure 3 shows the excitation number v and the maximal Lyapunov exponent λ_1 with varying T for the case of the activatory excitability. The excitation number is at the first glance a nondecreasing step-wise function of T (panel (a)) reflecting the gradually larger time for the system to recover before next pulse is delivered and hence more frequent excitations. Every p/q regime corresponds to a plateau. The blow-up in panel (b) shows that even a very narrow step between 1/3 and 1/2 resonances reveals fine step-wise structure but it also indicates that the value of v drops occasionally. More information provides the plot of λ_1. First of all, there are positive exponents (and hence chaotic dynamics) at some of the steps and second, these chaotic dynamical regimes occur predominantly where v drops. A similar picture emerges when the inhibitory excitable system is periodically perturbed.

The nature of chaotic attractors appearing in many windows is indicated in Fig. 4 showing phase portraits and Poincare sections taken successively at $t = kT$. The first case corresponds to the activatory excitability. The phase portrait (a) indicates the separating

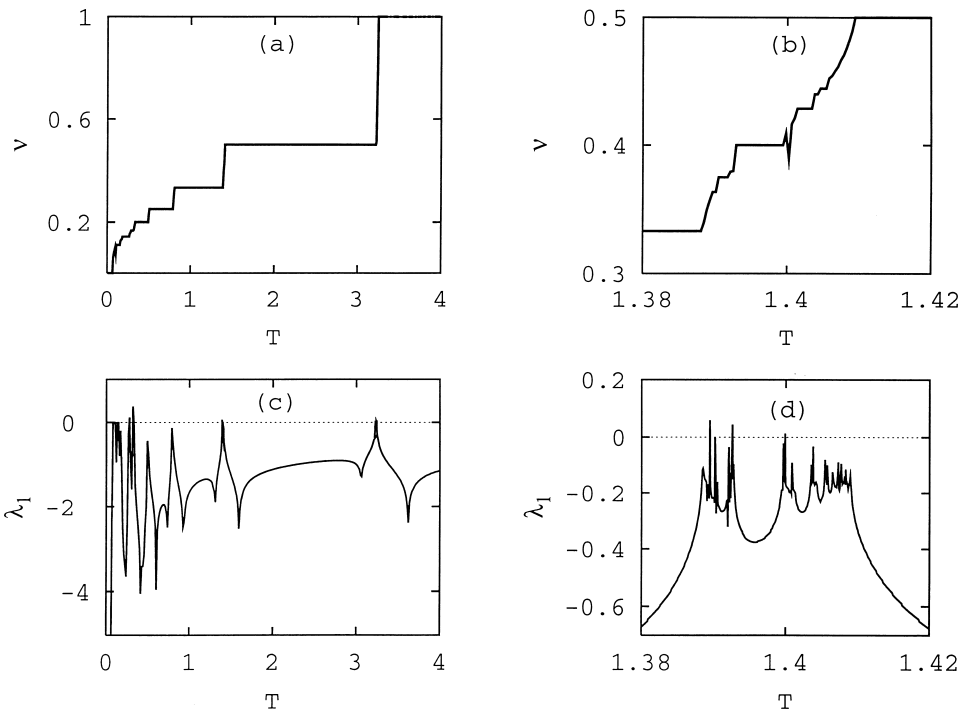

Fig. 3. Excitation number v and maximal Lyapunov exponent λ_1, against forcing period T, $v_0 = 1.2$, $A = 0.24$; (b) and (d) are enlarged portions of (a) and (c).

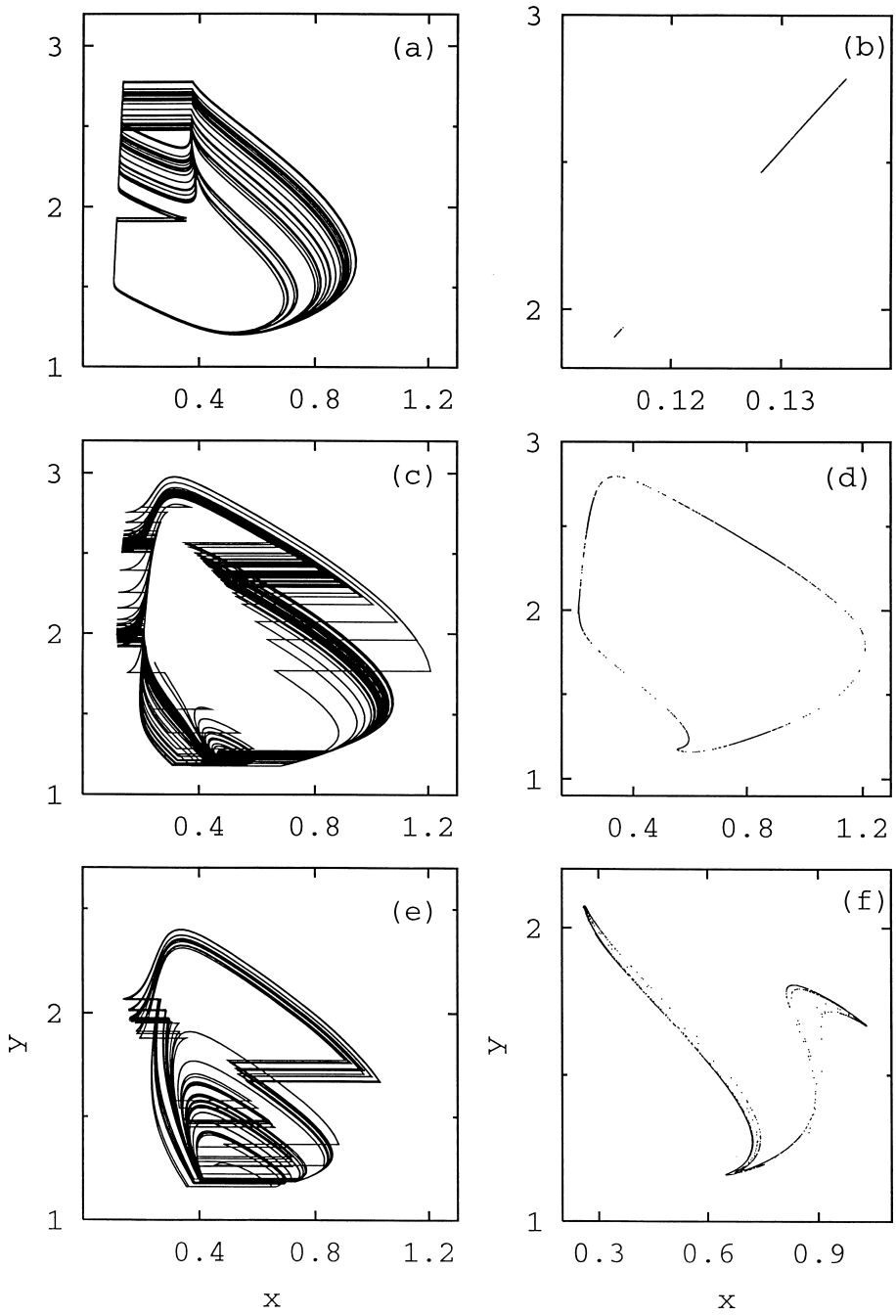

Fig. 4. Phase portraits (a), (c), (e) and Poincare plots (b), (d), (f) for three chaotic attractors; parameter values: (a), (b) $v_0 = 1.2$, $A = 0.24$, $T = 1.38945$, (c), (d) $v_0 = 5.0$, $A = 0.6$, $T = 0.2153$, (e), (f) $v_0 = 6.0$, $A = 0.6$, $T = 0.219$.

role played by the threshold set. On the other hand, the Poincare map (b) is extremely simple, suggesting that a 1D map is operating here. The second example (panels (c), (d)) is from the region of inhibitory excitability. The Poincare map (d) is, however, indicating that a fractalization of a torus leads to this attractor. The last example is showing an attractor with a well pronounced fractal structure which occurs when v_0 is selected closer to the boundary of vanishing inhibitory excitability.

2.4. Periodic forcing of two cells

Diffusion-coupled array of cells is the basic model for describing communication between cells via gap junctions where the simple diffusion driven interaction takes place. The interaction can only be mediated by cytosolic calcium Ca_i since the transport of sequestered calcium Ca_s is hindered. Taking the simplest possible array—two coupled cells—the Eqs. (1) and (2) extend to

$$\frac{dx_1}{dt} = f(x_1, y_1) + d(x_2 - x_1), \qquad \frac{dy_1}{dt} = g(x_1, y_1), \tag{10}$$

$$\frac{dx_2}{dt} = f(x_2, y_2) + d(x_1 - x_2), \qquad \frac{dy_2}{dt} = g(x_2, y_2), \tag{11}$$

where d is the transport coefficient.

We assume that cell 1 is periodically pulsed as before and examine how the excitation signal gets transferred to the second cell. The conditions in both cells are set either to activatory excitability (v_0 = 1.2) or to inhibitory excitability (v_0 = 5.0). The coupling strength has two obvious limits, when d is too small, no signal is propagated; when d is large enough, the cells fire synchronously. Depending on circumstances, the actual coupling strength may operate between the two limiting cases, in fact, this situation allows for a controlled way of signal transduction. We assume that the threshold set is not significantly altered by coupling and that the excitation numbers v_1, v_2 can be defined by counting the number of loops about the endpoint of the threshold set in each cell separately.

Adjusting the transport coefficient properly, complex dynamics is revealed by plotting v_1, v_2 and the maximal Lyapunov exponent λ_1 against T, see Fig. 5. The cases (a) and (c) correspond to the activatory excitability with d set to 6.0 and the cases (b) and (d) represent the dynamics of the inhibitory excitable system with d adjusted to 1.6; the forcing amplitude A is the same as for the corresponding one-cell systems. Excitation numbers in (a) show a complex pattern with mostly a partial propagation of the excitation to the second cell. The dominating pattern is 1:2 locking between the cells, only occasionally there is no propagation or complete propagation. Frequent drops of the staircase suggest possible chaotic dynamics which correspond well with positive λ_1 in (c). Panels (b) and (d) show essentially a similar pattern of alternating periodic and chaotic dynamics. However, there are some differences in the degree of synchronized firings—while for small T the two cells fire synchronously, for larger values the pattern alternates between no propagation and complete synchrony. This pattern cannot be made similar to that in (a) by adjusting d. This seems to reflect the difference between the activatory and inhibitory excitability.

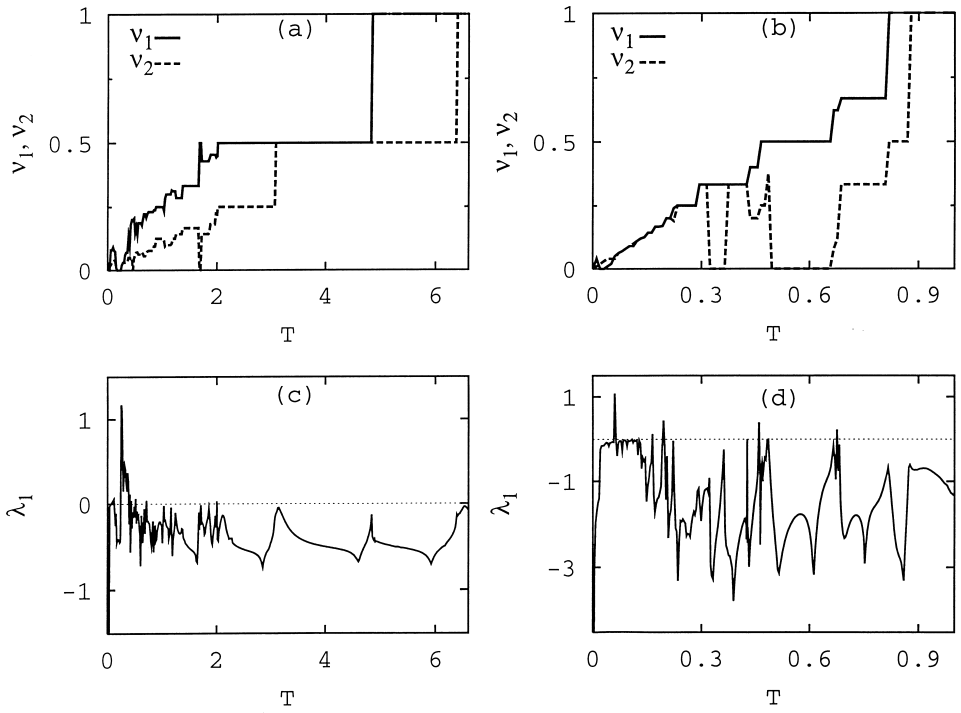

Fig. 5. Excitation numbers ν_1, ν_2 and maximal Lyapunov exponent λ_1 against forcing period T for two coupled cells; parameter values: (a), (c) $\nu_0 = 1.2$, $A = 0.24$, (b), (d) $\nu_0 = 5.0$, $A = 0.6$.

3. Chaotic Spatio-Temporal Patterns in Ca^{2+} Signalling System

In this section problems are analyzed associated with propagation of excitable pulse waves in spatially one-dimensional continuous medium, e.g., in a tissue formed by an assemblage of mutually coupled neural cells, where a part of the medium—*a pacemaker*—is set to the autonomous oscillatory state and the remainder of the system is in an excitable steady state making it capable of pulse wave transmission. The oscillating pacemaker perturbs (at its borders) the adjacent excitable regions and subsequently emits pulse waves into them. When no external fields affecting mass-transport rates in the system are present, the pacemaker emits the pulse waves symmetrically to both excitable regions. After the application of, e.g., electric field to the system, the symmetry is lost and one of the excitable regions communicates by pulse waves more frequently than the other one and also the spatial range of the signalling is changed. Here we address two particular topics of this signalling problem: The effects of the relative pacemaker size and of the intensity of electric field applied to the system on signalling behavior of the system. A transition from the periodic spatio-temporal signalling patterns to the chaotic ones is analyzed using the proper orthogonal decomposition (POD) based techniques.

3.1. Mathematical model

We consider a homogeneous one-dimensional reaction-diffusion medium as the environment where the calcium signalling takes place. First, the ICC kinetics of intracellular calcium oscillations is briefly introduced and then the signalling system model is constructed.

3.1.1. The ICC kinetics of intracellular calcium oscillations

The inositol 1, 4, 5-trisphosphate (IP_3)—calcium cross-coupling model (ICC) of calcium spiking in living cells (cf. MEYER and STRYER, 1991) belongs to the family of intracellular calcium kinetics models based on the receptor-controlled mechanism. The IP_3-Ca_i cross-coupling model of calcium spiking involves four variables: x, the concentration of Ca^{2+}, in the cell cytosol; y, the concentration of Ca^{2+} sequestered in the intracellular stores (endoplasmic and/or sarcoplasmic reticulum); u, the concentration of IP_3; and v, the fraction of active ionic channels through which the sequestered calcium is released from the intracellular stores into the cytosol. The evolution equations of the ICC model are (assuming well stirred reaction environment)

$$\frac{dx}{dt} = f_x = v\left[\frac{Au^4}{(u+K_1)^4} + L\right]y - \frac{Bx^2}{x^2+K_2^2}, \tag{12}$$

$$\frac{dy}{dt} = f_y = \frac{Bx^2}{x^2+K_2^2} - v\left[\frac{Au^4}{(u+K_1)^4} + L\right]y, \tag{13}$$

$$\frac{du}{dt} = f_u = C\left[1 - \frac{K_3}{(x+K_3)(1+R)}\right] - Du, \tag{14}$$

$$\frac{dv}{dt} = f_v = F_v(1-v) - E_v x^4 v. \tag{15}$$

The values of the kinetic parameters in Eqs. (12)–(15) used in numerical simulations reported in this paper are summarized in Table 2 (cf. MEYER and STRYER, 1991) together with other model parameters.

Table 2. Parameters of the ICC calcium signalling model.

Par.		Value		Par.		Value		Par.		Value	
A	=	20.0	s^{-1}	K_1	=	0.5	μM	Ev	=	1.0	$\mu M^{-4}\ s^{-1}$
B	=	40.0	$\mu M\ s^{-1}$	K_2	=	0.15	μM	Fv	=	0.02	s^{-1}
C	=	1.1	$\mu M\ s^{-1}$	K_3	=	1.0	μM	R	=	0.025	
D	=	2.0	s^{-1}	L	=	0.01	s^{-1}	x_0+y_0	=	1110.0	μM
R_{pac}	=	0.500		R_{exc}	=	0.025		D_x	=	0.5	$\mu m^2\ s^{-1}$
D_v	=	15	$\mu m^2\ s^{-1}$	z_x	=	+2		z_u	=	–6	
Z_l	=	100	μm	ε_p	...	variable		ε	...	variable	

3.1.2. The spatio-temporal ICC signalling system

The ICC kinetics of intracellular Ca^{2+} ions was assumed to take place within one-dimensional reaction-diffusion medium. The total length of the system Z_l was divided into oscillatory and excitable regions: The oscillatory region (pacemaker) was assumed to be located symmetrically around the center of the system with two excitable regions (of the same size) connected to its borders. The magnitude of the pacemaker region was expressed by its relative size $\varepsilon_p = Z_p/Z_l$, where Z_p is the pacemaker length. An electric field applied to the system boundaries was considered with the electric field intensity $\mathcal{E}$ constant throughout the system due to high ionic strength of the cytosol. The cytosolic Ca^{2+} ions (variable x) and cytosolic IP_3 ions (variable u) are considered as mobile components in our model and both the diffusion and electro-migration (described by the Nernst-Planck relation) are involved in their transport equations. The Ca^{2+} ions sequestered in the endoplasmic reticulum (variable y) and the ionic channels in the ER membrane (variable v) are taken as immobile components. The model equations (mass balances of signalling system components) can be found in HASAL *et al.*, 1996 and we thus omit them here. The values of model parameters used in our simulations are summarized in Table 2. Total length of the system considered in this paper is $Z_l = 100\ \mu$m.

The value of the parameter R (fractional activation of cell surface receptors) controls dynamical behaviour of the system: at low value ($R \leq 0.0258$) the ICC kinetics exhibits excitatory dynamics (cf., e.g., MEYER and STREYER, 1991; SCHREIBER *et al.*, 1999); autonomous oscillations take place in stirred environment when $R > 0.02568$ with the period decreasing with the increasing R (see SCHRE1BER *et al.*, 1999). The value of the parameter R was set to $R_{pac} = 0.500$ and to $R_{exc} = 0.025$ for the oscillatory and the excitable regions, respectively. The relative pacemaker size ε_p, and applied electric field intensity $\mathcal{E}$ were considered as adjustable parameters of the ICC signalling system.

3.2. Characterization of spatio-temporal signalling patterns

The technique of *proper orthogonal decomposition* (POD) is being increasingly used as a tool for analysis and characterization of spatio-temporal chaotic patterns. We shall in the following describe the use of the POD and the computation of the entropy-like quantities for both the qualitative and quantitative characterization of chaotic spatio-temporal patterns emerging in the signalling system described above.

The POD (BROOMHEAD and KING, 1986; KOLODNER *et al.*, 1995) decomposes spatio-temporal pattern $u(z, t) = U(z, t) - \overline{U}(z)$, where $\overline{U}(z)$ is temporal average of $U(z, t)$, into a set of spatial eigenmodes $\Phi_i(z)$ called *topos* and of temporal eigenmodes $a_i(t)$ called *chronos* or amplitudes

$$u(z,t) = \sum_{i=1}^{N} \Phi_i(z) a_i(t). \tag{16}$$

The spatial eigenmodes $\Phi_i(z)$ are solutions of the eigenvalue problem

$$C\Phi_i = \alpha_i \Phi_i, \qquad (i = 1, 2, \ \ldots, \ N) \tag{17}$$

where α_i are eigenvalues associated with the individual spatial eigenmodes Φ_i and the

kernel C = C(z, z') is a two-point spatial correlation matrix of the pattern $u(z, t)$ (cf. HASAL *et al.*, 1996). The temporal eigenmode (chronos) is evaluated as inner product of the spatial eigenmode Φ_i with the pattern $u(z, t)$

$$a_i(t_k) = (u(z,t_k).\Phi_i(z)) = \sum_{j=1}^{N} u(z_j,t_k)\Phi_i(z_j) \quad i = 1,2,\ \ldots,\ \mathrm{N}; k = 1,2,\ \ldots,\ \mathrm{M} \tag{18}$$

Quantities averaging system dynamics either over the time or the space domain alone, so called *spatial entropy* $H_s(t)$ and *temporal entropy* $H_T(z)$, respectively (KOLODNER *et al.*, 1995) are used to characterize temporal or spatial complexity of the spatio-temporal patterns. The spatial entropy is defined as

$$H_S(t) = -\frac{1}{\log N}\sum_{i=1}^{N} p_{a_i}(t)\log p_{a_i}(t), \quad \text{where} \quad p_{a_i}(t) = \frac{\alpha_i |a_i(t)|}{\sum_{j=1}^{N}\alpha_j |a_j(t)|}. \tag{19}$$

The temporal entropy is given by

$$H_T(z) = -\frac{1}{\log N}\sum_{i=1}^{N} p_{\Phi_i}(z)\log p_{\Phi_i}(z), \quad \text{where} \quad p_{\Phi_i}(z) = \frac{\alpha_i |\Phi_i(z)|}{\sum_{j=1}^{N}\alpha_j |\Phi_j(z)|}. \tag{20}$$

3.3. Effects of pacemaker size on the ICC signalling patterns

The spatio-temporal patterns of the cytosolic calcium concentration x originating from mutual interaction of the oscillatory pacemaker with the adjacent excitable regions in the ICC Ca^{2+} signalling system are depicted in Fig. 6 where traces of the maxima of $x(z, t)$ are plotted for various relative pacemaker sizes ε_p at fixed pacemaker frequency (given by the R_{pac} value). No electric field is applied in Fig. 6. The spatio-temporal dynamics of the system undergoes substantial variations when the pacemaker size is varied: The small pacemaker (ε_p = 0.008) performs simple period 1 (P1) oscillations and each pacemaker oscillation evokes a pair of excitable pulses propagating with the same speed through both excitable regions. However, each second pulse pair dies out before it reaches the system boundaries. The larger pacemaker (ε_p = 0.042) performs periodic oscillations with periodicity P13. Two distinct firing patterns alternate in Fig. 6c: the pattern 1:5 (i.e. each fifth pacemaker oscillation evokes a pair of the excitable pulses) and the pattern 1:8 (cf. also respective phase plot in Fig. 6). The excitable pulses propagate with the same speed and the resulting spatiotemporal pattern is symmetric around the system axis. The pacemaker with relative size ε_p = 0.100 oscillates with high periodicity Pn (n = 30).

The structure of the inner spatio-temporal pattern within the pacemaker regions begins to be complex and results in a large number of short-distance propagating pulse waves fastly vanishing in the excitable regions. The symmetry of the spatio-temporal pattern is partly lost when large pacemaker is located in the signalling system (ε_p = 0.200 and 0.400). The pacemaker oscillations become chaotic (see phase plots in Figs. 6d, e) and the pulse waves are not emitted synchronously to both excitable regions. The structure of the spatio-

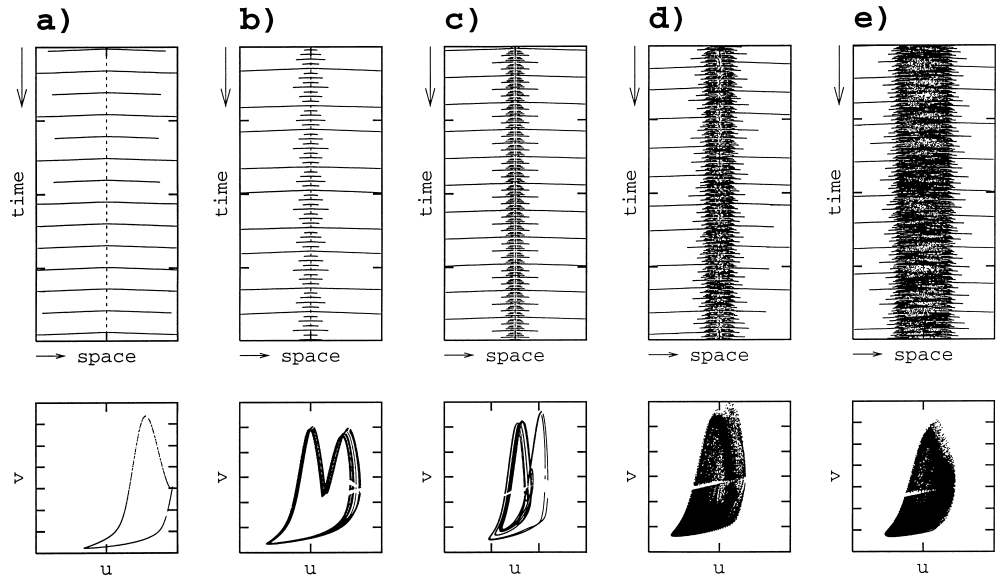

Fig. 6. Spatio-temporal patterns in ICC calcium signalling system (upper panels, spatial range 0–100 μm, time range 500 min, traces of maxima of cytosolic Ca^{2+} are plotted) and phase portraits of system trajectory recorded at $z = Z_l/2$ (lower panels). Relative pacemaker size: a) $\varepsilon_p = 0.008$; b) $\varepsilon_p = 0.042$; c) $\varepsilon_p = 0.100$; d) $\varepsilon_p = 0.200$; e) $\varepsilon_p = 0.400$. Electric field intensity $\mathcal{E} = 0$ Vcm^{-1}.

temporal pattern within the pacemaker with $\varepsilon_p = 0.200$ is shown in Fig. 7a. The traces clearly document complex structure of the pattern with the waves irregularly moving forth and back within the pacemaker region. Wave splitting, annihilation and propagation direction reversal can be detected in Fig. 7a. The pulse waves emitted to the excitable regions originate mostly from interactions of system regions with the distinct dynamics at the pacemaker-excitable region interface.

The leading spatial POD eigenmodes—the topos—at various intensity of the electric field are depicted in Fig. 8. Almost perfect spatial symmetry of the topos is apparent that results from the system symmetry when no electric field is applied. The spatial symmetry of the pattern is reflected also in the profiles of the temporal entropy $H_T(z)$ in Fig. 9. The entropy production rate is quite uniformly distributed across the system at the pacemaker size below $\varepsilon_p < 0.100$. There is only a shallow minimum of the $H_T(z)$ in the pacemaker region where the system performs more or less periodic motions. The $H_T(z)$ is also lowered close to the system boundaries where the pulse waves vanish. The pacemaker region exhibits significantly suppressed entropy production for large pacemakers ($\varepsilon \leq 0.100$).

3.4. Electric field control of the ICC signalling dynamics

The effects of the electric field on the intrinsic patterns in the pacemaker region are shown in Fig. 7b. Two principal consequences of the electric field action are evident: The propagation of the pulse waves against the direction of the electric field is suppressed and the intra-pacemaker pattern becomes more regular.

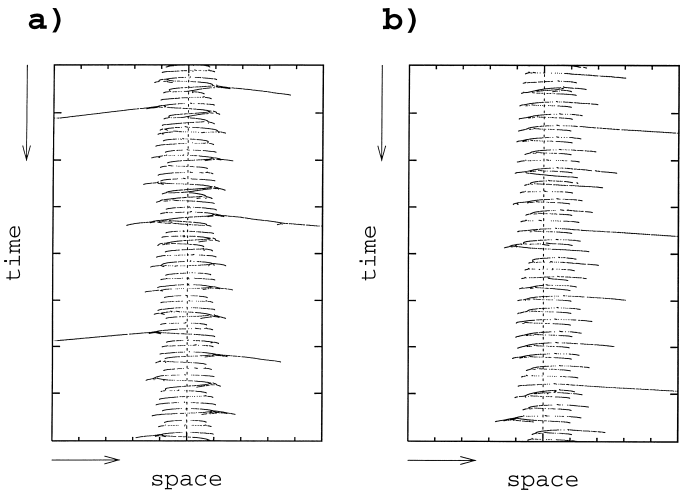

Fig. 7. Effects of electric field intensity on spatio-temporal patterns in ICC calcium signalling system. a) $\mathcal{E}$ = 0 Vcm^{-1}, b) $\mathcal{E}$ = 10 Vcm^{-1}. Relative pacemaker size ε_p = 0.200. The traces of maxima of cytosolic Ca^{2+} concentration are plotted. Spatial range: 0–100 μm; time range: 150 min.

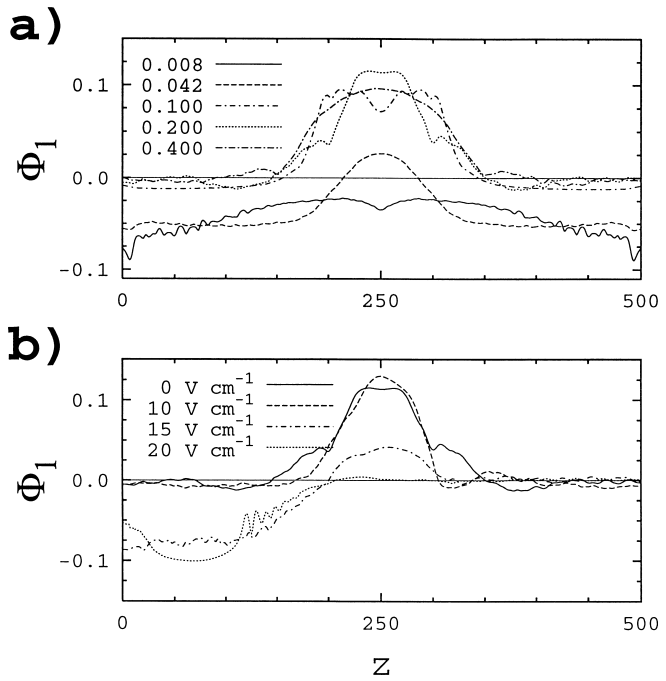

Fig. 8. Dominant topos Φ_1 of chaotic upatterns in ICC calcium signalling system. a) Effects of the pacemaker relative size (at electric field intensity $\mathcal{E}$ = 0 Vcm^{-1}), b) effects of electric field intensity (at relative pacemaker size ε_p = 0.200).

The electric field applied to the ICC signalling system elicits strong spatial asymmetry of the signalling pattern generated in the system. This fact is clearly evident from the shape of the first three leading topos of the signalling pattern (see Fig. 9b). The asymmetry arises due to the different mobilities of both mobile components of the ICC model (positive Ca^{2+} ions and negatively charged IP_3). The electric field also strongly influences the entropy production rate in the system (Fig. 9b). The entropy production is supressed in the part of the system where the pulse waves do not propagate.

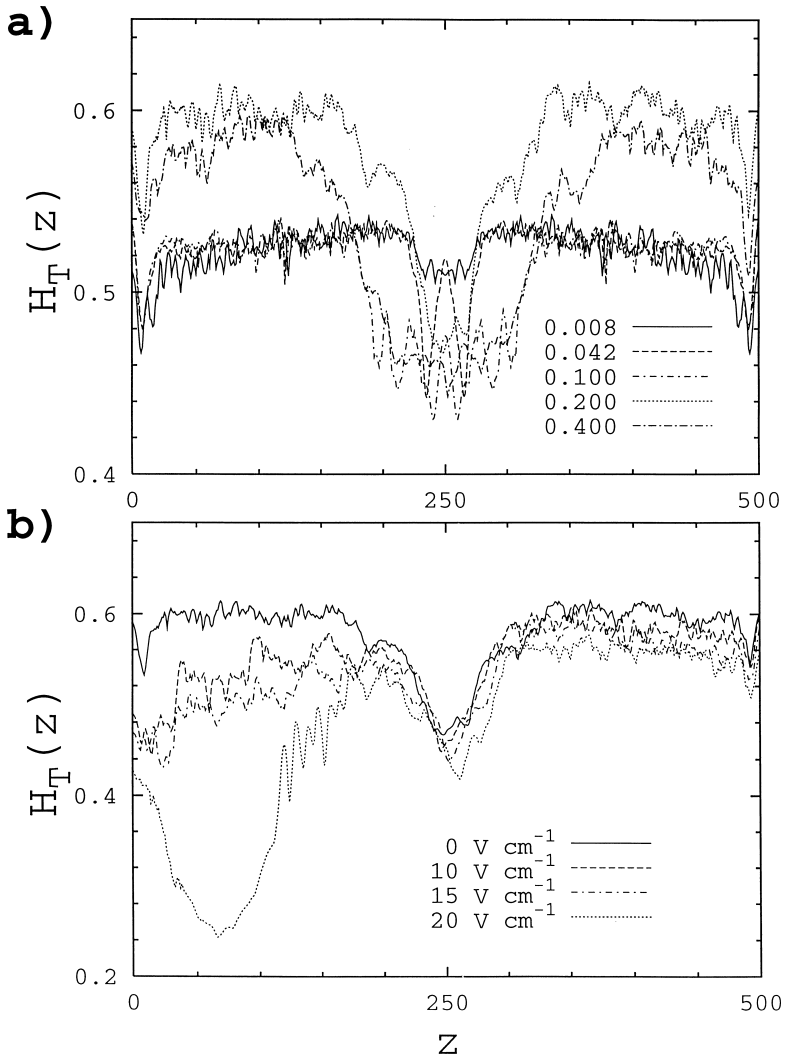

Fig. 9. Spatial distribution of temporal entropy $H_T(z)$ in ICC calcium signalling system, a) Effects of the pacemaker relative size; electric field intensity $\mathcal{E} = 0$ Vcm^{-1}), b) Effects of electric field intensity; relative pacemaker size $\varepsilon_p = 0.200$.

4. Conclusions

It is shown that complex dynamic patterns occur even in the simplest case of one periodically pulsed excitable cell and they are associated with localized drops of the staircase-like dependence of excitation number on forcing period. In an array of two cells spatio-temporal structures of partially propagated pulses occur for intermediate coupling strengths and chaotic regimes are again associated with drops of the excitation number when the forcing period is increased.

Spatio-temporal calcium signalling patterns in a spatially continuous environment develop from simple pairs of pulse waves periodically emitted from the pacemaker to complex time-periodic structures leading eventually to spatio-temporally chaotic patterns when the relative pacemaker size is increased. The signalling patterns become more organized under the influence of external electric field imposed to the system.

Calcium dynamics in cytosol is one of many distinct signalling pathways. Components of different pathways interact resulting in signalling networks with emergent properties such as welldefined input thresholds, bistability and signal modulation in response to stimuli (BHALLA and IYENGAR, 1999). Methods of analysis presented in this paper are well suited for investigating dynamics in this more complex situation.

The authors thank to the Grant Agency of Czech Republic (Grant No. 203/98/1304) and to the Ministry of Education of Czech Republic (Grant VS96073) for the financial support of this project.

REFERENCES

BERRIDGE, M. J., BOOTMAN, M. D. and LIPP, P. (1998) Calcium—a life and death signal, *Nature*, **395**, 645–648.

BOITANO, S., DIRKSEN, E. R. and SANDERSON, M. J. (1992) Intercellular propagation of calcium waves mediated by inositol trisphosphate, *Science*, **258**, 292–295.

BHALLA, U. S. and IYENGAR, R. (1999) Emergent properties of networks of biological signaling pathways, *Science*, **283**, 381–387.

BROOMHEAD, D. S. and KING, G. P. (1986) Extracting qualitative dynamics from experimental data, *Physica*, **D20**, 217–236.

CAPLAN, S. R., NAPARSTEK, A. and ZABUSKY, N. J. (1973) Chemical oscillations in a membrane, *Nature*, **245**, 364–366.

COOPER, M. S. (1995) Intercellular signaling in neuronal-glial cells, *BioSystems*, **34**, 65–85.

DUPONT, G. and GOLDBETER, A. (1993) One-pool model for Ca^{2+} oscillations involving Ca^{2+} and inositol 1, 4, 5—trisphosphate as co-agonists for Ca^{2+} release, *Cell Calcium*, **14**, 311–322.

FIELD, R. J. and BURGER, M., eds. (1990) *Oscillations and Travelling Waves in Chemical Systems*, Wiley, New York.

GOLDBETER, A. (1996) *Biochemical Oscillations and Cellular Rhythms*, Cambridge University Press, Cambridge.

HASAL, P., NEVORAL, V., SCHREIBER, I., ŠEVČÍKOVÁ, H., ŠNITA, D. and MAREK, M. (1996) Waves in ionic reaction-diffusion-migration systems, in *Nonlinear Dynamics, Chaotic and Complex Systems* (eds. E. Infeld *et al.*), Cambridge Univ. Press, Cambridge.

HODGKIN, A. L. and HUXLEY, A. F. (1954) A quantitative description of membrane current and application to conduction and excitation in nerve, *J. Physiol.*, **117**, 500–544.

HOLDEN, A. V., MARKUS, M. and OTHMER, M. G., eds. (1991) *Nonlinear Wave Processes in Excitable Media*, Plenum Press, New York.

KUBÍČEK, M. and MAREK, M. (1983) *Computational Methods in Bifurcation Theory and Dissipative Structures*, Springer, New York.

KOLODNER, P., SLIMANI, S., AUBRY, N. and LIMA, R. (1995) Characterization of dispersive chaos and related states of binary-fluid states, *Physica*, **85**, 165–224.

MAREK, M., FINKEOVÁ, J. and SCHREIBER, I. (1989) Devil's staircase in chemical excitable systems, in Workshop "Irreversible Processes and Selforganization" (ed. W. Ebeling), Teubner Verlag, Leipzig, pp. 76–79.

MAREK, M. and SCHREIBER, I. (1995) *Chaotic Behaviour of Deterministic Dissipative Systems*, Cambridge University Press, Cambridge.

MEYER, T. and STRYER, L. (1991) Calcium spiking, *Ann. Rev. Biophys. Biophys. Chem.*, **20**, 153–174.

SCHREIBER, I., HASAL, P. and MAREK, M. (1999) Chaotic patterns in a coupled oscillator–excitator biochemical cell system, *CHAOS*, **9**, 43–54.

VOTRUBOVÁ, V., HASAL, P., SCHREIBEROVÁ, L. and MAREK, M. (1998) Dynamical Patterns in Arrays of Coupled Chemical Oscillators and Excitators, *J. Phys. Chem. A*, **102**, 1318–1328.